Available online at www.sciencedirect.com
ScienceDirect
Earth and Planetary Science Letters 248 (2006) 830–839
EPSL
www.elsevier.com/locate/epsl

Elastic thickness estimates for the northern lowlands of Mars

Trudi Hoogenboom *, Suzanne E. Smrekar

Jet Propulsion Laboratory, California Institute of Technology, 4800 0ak Grove Drive, Mail Stop 183-501, Pasadena, CA 91109, United States

Received 22 March 2006; received in revised form 19 June 2006; accepted 23 June 2006
Available online 24 July 2006
Editor: Scott King

Abstract

The northern lowlands cover approximately one-third of Mars' surface and are a fundamental part of the geologic evolution of Mars. We examine the admittance signature, the ratio of gravity to topography data in the spectral domain, for four regions in the northern lowlands that are both well resolved in the gravity data and have well constrained lithospheric parameters. These regions also have topographic power spectra similar to many highlands regions. A Cartesian multitaper method is used to calculate admittance. We compare the observed admittance signatures to those predicted from models of lithospheric flexure. On the basis of these comparisons, we estimate the thickness of the Martian elastic lithosphere (T_e) required to support the observed topographic load since the time of loading. We use both top and bottom loading models to derive values of elastic thickness and crustal thickness or apparent depth of compensation although all four regions are best fit by bottom loading models. We obtain best fit elastic thickness estimates between 10 and 25 km with an acceptable error range of 0 to 45 km. These low elastic thickness estimates are consistent with the formation in the Noachian, when heat flow was high. The consistency in T_e estimates between the Noachian highlands and lowlands basement suggests that both regions of the crust formed at similar times. The paucity of crustal magnetization in the lowlands is thus more likely a result of demagnetization than formation following shut down of the dynamo.

Keywords: Mars; elastic thickness; northern lowlands; admittance

1. Introduction

The hemispheric dichotomy of Mars is one of the most prominent topographic structures on the planet and is defined by the relatively smooth northern plains and the heavily cratered southern highlands. Various mechanisms have been proposed to explain the fundamental differences in terrain between the two hemispheres including internal processes related to mantle convection [1–3] and external processes related to one or more large impacts [4,5]. The lowlands may have contained a large body of standing water early in Mars' history [6,7] and have also been proposed to be the location of plate tectonic activity in earliest Mars history [8]. In this study we estimate elastic thickness, crustal thickness and apparent depth of compensation for regions of the northern lowlands of Mars to better constrain the timing of the northern lowlands formation or other major loading events.

Topography and gravity measured by the Mars Global Surveyor have enabled the determination of the global crust and upper mantle structure of Mars [e.g. 9–13]. However, there have been no successful estimates of

* Corresponding author. Present address: ExxonMobil Exploration Company, Technology/Geophysical Operations, CORP-GP8-688B.
E-mail address: Trudi.M.Hoogenboom@exxonmobil.com (T. Hoogenboom).

0012-821X/$ - see front matter © 2006 Elsevier B.V. All rights reserved.
doi:10.1016/j.epsl.2006.06.035

elastic thickness in the northern lowlands (with the exception of Utopia basin [14]) due to low topographic signal. We use a multitaper approach (that has been successful for analogous regions on Earth [15]) to estimate elastic thickness.

2. Gravity and topography data

We use gravity data computed from the latest spherical harmonic field (MGS95J) [16], carried out to spherical harmonic degree and order 95. The gravity field is determined globally to about degree 70 (~305 km), where the "noise" or uncertainties of the unconstrained solution equals the "signal" or magnitude of MGS95J. The improvement in this gravity field comes from additional tracking data and the adoption of a more complete Mars orientation model [16]. The resolution of the gravity field is predominantly a function of spacecraft altitude. An approximate measure of the resolution of the data is given by the degree strength. The degree strength is the local degree and order of the field where the amplitude of the noise is equal to the strength of the signal. The choice of maximum cut-off degree for geophysical modeling involves a trade-off between resolution and uncertainty.

Spherical harmonic coefficients for the topography field have been created by the MOLA team in the same reference as the gravity field [17]. As the topography field is far more accurate than the gravity field, errors in topography are ignored. We projected the topography and gravity data in GMT using an equal area Hammer projection [18]. The data was then regrided to be equally spaced at 59.2 km intervals (~equivalent to 1° in latitude).

3. Method

Flexural compensation assumes that loads are partly supported by stresses within the elastic lithosphere and partly by buoyancy anomalies generated by deflection of the lithosphere. The relative importance of isostasy versus flexural deflection in compensating loads at a given wavelength depends on the flexural rigidity of the elastic plate, D:

$$D = \frac{ET_e^3}{12(1-\upsilon^2)} \tag{1}$$

where, E is Young's modulus (10^{11}) and υ is Poisson's ratio (0.25). A large T_e corresponds to a strong lithosphere in which elastic stress supports a significant fraction of loading. Small T_e implies relatively little elastic support of stress.

We estimate T_e using free-air admittance. We first calculate the observed admittance and then compare it to admittance predicted for a range of T_e values. Surface and subsurface loads are deconvolved from the data for a given T_e and admittance is then calculated assuming that the loads are statistically uncorrelated [19]. The best fit T_e estimate is that which yields a minimum root-mean-square error between the observed and predicted admittance.

3.1. Admittance

The admittance method examines the relationship between gravity and topography in the spectral domain [19], and is sensitive to elastic thickness because the T_e controls the response of the surface to loads of a given size. The admittance $Q(k)$, is defined as the transfer function between the spectral representation of the gravity, $G(k)$, and topography, $H(k)$, and assumes that the lithosphere is laterally isotropic

$$G(k) = Q(k)^* H(k) + N(k) \tag{2}$$

where k is the two-dimensional wave number, $2\pi/\lambda$, and λ is the wavelength [20]. $N(k)$ is the noise in the data, which is assumed to be small. Data are averaged over discrete wave number bands to prevent bias by noise. The admittance estimate is written as:

$$Q(k) = \frac{\langle GH^* \rangle}{\langle HH^* \rangle} \tag{3}$$

with angle brackets indicating averaging over wave number bands and the asterisk denotes the complex conjugate.

3.2. Multitaper windowing scheme

In the determination of lithosphere thickness, the northern lowlands of Mars represent a special case because deposition and erosion have smoothed the topography locally to such an extent that inversions based on admittance methods yield biased results [19]. A similar situation occurs for many terrestrial continental regions e.g. Australia, where erosion or infilling has leveled the topography on a regional scale. Swain and Kirby [15] investigate this problem in detail. Using synthetic models of topography and surface and subsurface loads, they create synthetic topography and gravity with power spectra very similar to those computed for the Australian continent, which they refer to as a "low" signal to noise example. Across the wavelength range we examine (400–1900 km), our regions (Fig. 1) display a similar relative range of topographic power amplitude (~1.3–1.4 $\log_{10}$ units) when

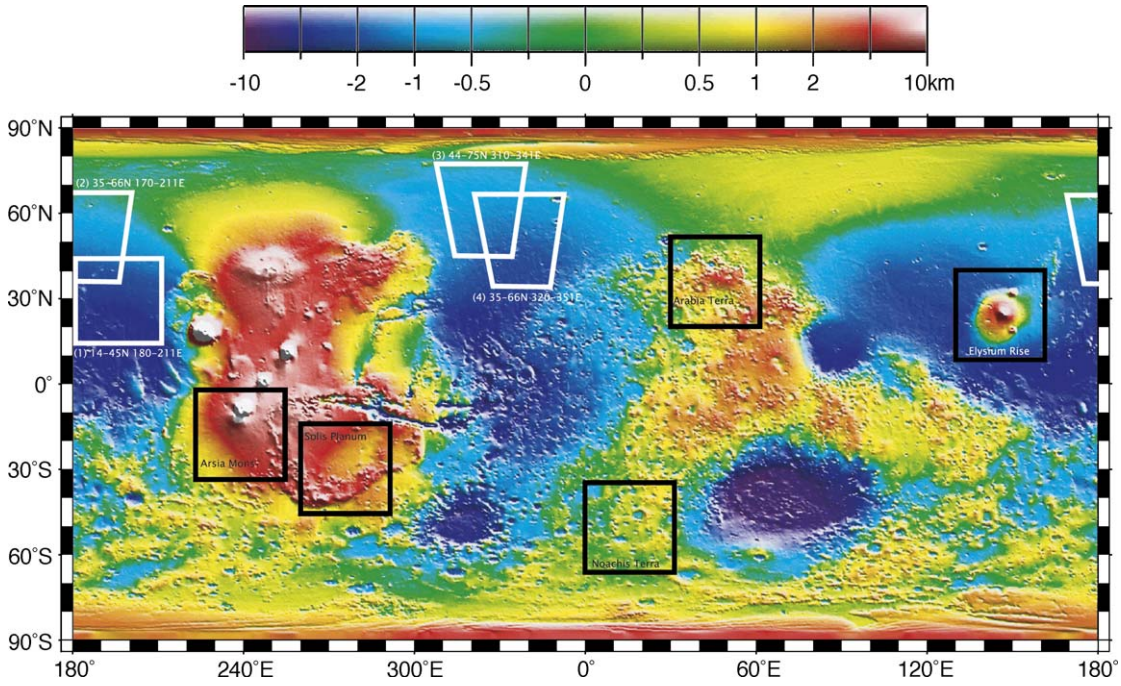

Fig. 1. Locations of the 4 northern lowlands regions are outlined in white on the MOLA topography. Locations of southern highland regions used to compare topographic power in Fig. 2 are shown in black.

compared with the relative range of topographic power of Australia [15] (1.2 $\log_{10}$ units) and other eroded terrestrial cratons (1.4 $\log_{10}$ units) [e.g. 21]. Swain and Kirby [15] also create a 'normal' S/N example, in which the ratio of bottom to surface loads is 1. They estimate the bias introduced into the admittance when the topographic signature is low and find that the estimates are quite accurate for low values of T_e, e.g. $T_e \leq 40$ km, but T_e is underestimated for larger T_e values.

Following the approach of Swain and Kirby [15], we use a multitaper spectral estimation technique [22]. In this approach, we apply a fast Fourier transform to square regions ($\sim 1900 \times 1900$ km) to examine their spectral signature. The multitaper method windows the data with a set of orthogonal functions. In this study we use discrete prolate–spheroidal sequences [23]. The final, minimum bias spectrum at each wave number (k_x, k_y) is a weighted average of the spectra generated for each of the individual tapers. The multitaper estimator reduces the variance of the spectral estimate and also defines the spectral resolution [24].

We set the bandwidth parameter NW to 3, where N is the number of samples in the series and W is the half bandwidth of the central lobe of the power spectral density of the tapers (see, e.g. [25]). The choice of NW is important in the calculation of T_e [26]. As the bandwidth increases, the resolution (i.e. the minimum separation in wave number between approximately uncorrelated spectral estimates) decreases [27]. Similar to Perez-Gussinye et al. [26], we found that smoother admittance spectra with smaller model fit errors were obtained using 3 lower order tapers as compared to 2, 4 or 5 tapers.

To test the validity of the multitaper approach, we estimated T_e for a range of features in the southern highlands of Mars (e.g. Hellas Basin, Noachis Terra, NE Arabia Terra, Solis Planum and Ascraeus Mons) which have been previously studied [9,11]. The estimates obtained were generally within 1.5 times the RMS misfit of those obtained in previous studies.

3.3. Elastic compensation models

Standard bottom loading and top loading models were used to fit the observed admittance signature for each region. For all models, a crustal density of 2900 kg/m^3 (intact basalt) and a mantle density of 3500 kg/m^3 are assumed. Following Neumann et al. [28] and Wieczorek and Zuber [29] (who estimated the average thickness of the Martian crust to lie between 33 and 81 km), a 50 km thick Martian crust is assumed in the bottom loading fits and the elastic thickness and apparent depth of compensation (Z_L or ADC) are estimated.

The standard transfer function for top loading of the elastic lithosphere from above was developed by Banks et al. [30]

$$Q_{\mathrm{T}}(k) = 2\pi\rho_c G\left[\frac{1-\exp^{-\mathrm{k}Z_c}}{\left(1+\frac{Dk^4}{\Delta\rho g}\right)}\right] \quad (4)$$

where G is the gravitational constant, Z_c is the thickness of the crust, g is the gravity, D is the flexural rigidity and $\Delta\rho$ is the density contrast at the crust mantle boundary, or the difference between, ρ_m, the mantle density, and ρ_m, the crustal density. Note that the equations given here are for free-air gravity.

For bottom loading at depth [31], the admittance is defined as:

$$Q_N = 2\pi G\left\{\rho_c + (\rho_m-\rho_c)\exp^{-\mathrm{k}Z_c} - \left[(Dk^4+\rho_m g)/g\right]\exp^{-\mathrm{k}Z_L}\right\} \quad (5)$$

We include a second compensation depth, Z_L, below the crust mantle boundary interface which is assumed to represent the density difference near the base of the thermal lithosphere.

3.4. Estimation of error

Error estimates are used to constrain the range of model parameters that provide a reasonable fit to the data. The root-mean-square (RMS) formula is used to compare the observed and predicted admittance, with the RMS misfit given as

$$RMS_{\mathrm{fit}} = \left\{\frac{1}{N}\Sigma\left[\frac{(Z_{obs}-Z_{prd})^2}{\Delta Z_s}\right]\right\}^{\frac{1}{2}} \quad (6)$$

where N is the number of admittance values in the spectrum, Z_{obs} is the observed admittance, Z_{pred} is the predicted model admittance, and ΔZ_s is the RMS of the error in the admittance spectra calculated at each wave number band [21]. We estimate the allowable range of lithospheric parameters to be those that have a model fit RMS error ≤ 1.5 times the average admittance uncertainty for each region. The allowed parameter ranges that result from choosing an error 2 times the observed RMS, vary from slightly larger than those for a factor of 1.5 to a factor of 2 larger.

Each spectrum is fit over the wavelength range defined by the degree strength (at the short wavelength end) and the box size. Models were run using T_e values of 0–100 km at 5 km increments, Z_C, values of 0–100 km at increments of 5 km, and Z_L values from 30 to 200 km, at 10 km increments.

4. Results

McGovern et al. [9] found large fluctuations in the admittance spectra in the northern lowlands. They attributed this behavior to subsurface loads that are uncorrelated with the topography and low topographic power. We systematically compared the power in the topography across $\sim 1900\times 1900$ km regions in the northern lowlands and found that the majority of lowland regions exhibit low topographic power; resulting in noisy admittance spectra or large model fit errors. McGovern et al. [9,10] found a similar result. However, four northern lowlands regions (shown in Fig. 1) had comparable topographic power to regions in the southern highlands previously used to calculate elastic thickness [e.g. 9] (Fig. 2). These regions also displayed smooth admittance signatures (less than 15 mgal/km variation across the wavelength range we examine) and well constrained lithospheric parameters. We tested the effect of box size on the observed admittance and found that using regions larger than 1900 km in the east-west direction did not increase the topographic power or significantly affect the admittance signature. The north-south dimension of the box could not be increased without including either the southern highlands or the polar caps. These windows are much larger than the true flexural wavelength and are thus adequately sized to capture the flexural signature [15]. We note that although there is an overlap between these regions, we analyze the signature of all four areas to maximize the possible coverage of the northern plains.

The relative variation in topography within each region ranges from 2 to 2.25 km. A summary of the best fitting parameter values (T_e, Z_c and Z_L) for all 4 regions is given in Table 1. All four regions were best fit by a bottom loading model resulting in T_e estimates between 0 and 45 km for region 1 (Amazonis Planitia), 0 and 23 km for region 2 (Arcadia Planitia), 13 and 30 km for region 3 (Acidalia Planitia-A) and 0 to 30 km for region 4 (Acidalia Planitia-B). Z_L estimates ranged between 64 and >150 km for region 1, 100 and 140 km for region 2, 85 and 115 km for region 3 and 30 to 87 km for region 4. In each of these four regions, we were unable to obtain an acceptable fit (<15 mgal/km) using a top loading model. The best fit top loading models displayed minfit errors of 16.7, 19.7, 33.1 and 22.8 mgal/km for regions 1 though 4 respectively. We display contours of RMS misfit on a two-parameter projection of the chosen parameter space (Fig. 3e,f,g,h). Models having large RMS fit errors were rejected. The solid vertical line in Fig. 3a, b,c,d represents the limit of the resolution of the gravity field ($\sim$305 km).

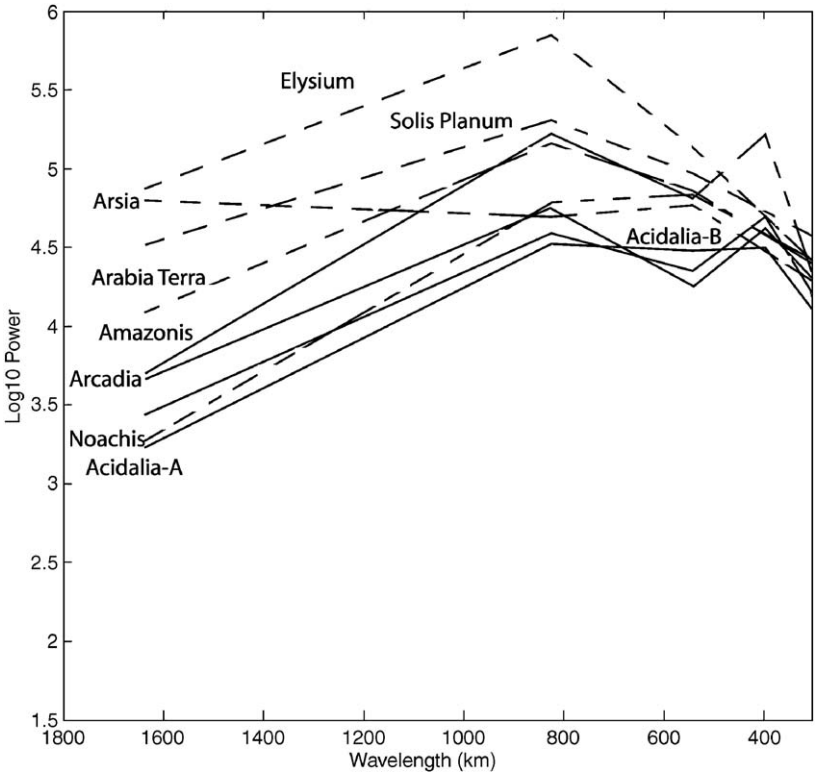

Fig. 2. Multitaper (NW=3) power spectra of topography data for 5 regions in the southern highlands (dashed lines) and 4 regions in the northern lowlands (solid lines). All data-sets are (~1900×1900 km).

Many of the remaining areas in the northern highlands for which we were unable to fit an elastic model (due to low power in the topography) displayed admittance signatures with shapes similar to those displayed in Fig. 3a,b,c,d,e,f. We did not examine the Utopia basin region as large basins typically require either forward modeling [e.g. 14] or finite amplitude modeling [e.g. 32] to accurately estimate T_e.

4.1. Coherence

The coherence method [19] calculates the statistical correlation between gravity and topography and has been widely used to estimate the effective elastic thickness of the continental lithosphere. In the coherence method, elastic thickness and $f(k)$ are determined iteratively where f is the ratio of the magnitude of the bottom load to the top load. Currently, the gravity data quality on Mars is such that coherence analysis cannot be used to constrain the loading mechanism and elastic thickness. However, McGovern et al. [10] suggest that coherence values >0.5 imply that admittance analysis is a viable alternative. We have calculated and modeled the coherence and found that the coherence for our study areas meet this criteria (Fig. 3i,j,k,l). The coherence for region 4 is

Table 1
Estimated lithospheric parameters, observed error in the admittance and the misfit between the observed and predicted admittance for 4 regions in the northern lowlands

Region	Projection	Best fit T_e (km)	T_e range (1.5) (km)	Best fit Z_L (km)	Z_L range (1.5) (km)	Obs. error (mgal/km)	Fit error (mgal/km)
1. Amazonis Planitia 14–45N 180–211E	–	25	0–45	100	64–>150	6.36	12.29
2. Arcadia Planitia 35–66N 170–201E	Hammer equal area	10	0–23	120	100–140	11.94	6.29
3. Acidalia Planitia-A 44–75N 310–341E	Hammer equal area	25	13–30	100	85–115	4.69	10.0
4. Acidalia Planitia-B 35–66N 320–351E	Hammer equal area	20	0–30	50	30–87	7.06	11.49

Allowable ranges T_e and Z_L are shown for RMS values of 1.5 times the observed RMS error. All four regions were best fit by a bottom loading model. In each case the crustal thickness was set to 50 km.

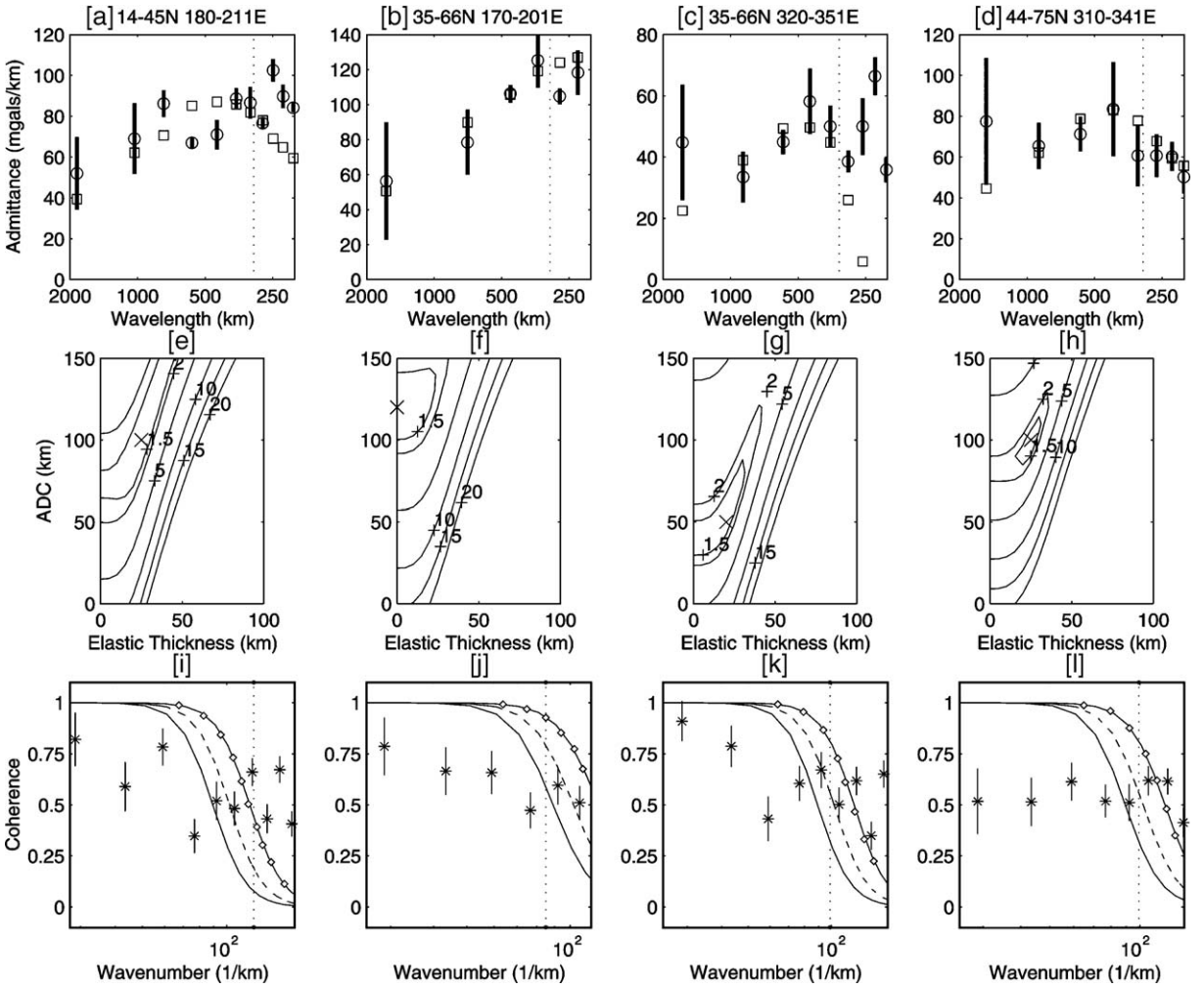

Fig. 3. Cartesian admittance spectra versus wavelength for the four northern lowland regions: (a) 14–45N 180–211E, (b) 35–66N 170–211E, (c) 44–75N 310–341E and (d) 35–66N 320–31E. The resolution cut-off of the gravity data is indicated by a vertical line. For each region the observed admittance is shown by circles. Vertical solid lines represent the observed admittance error. Squares show the model admittance. RMS model errors (mgal/km), for each region are shown in Fig. 3 (e,f,g,h). The model with the minimum error is marked by an 'X'. Fig. 3 (i,j,k,l) shows the observed and modeled coherence for each region. The observed coherence and error is indicated by the asterisks and vertical lines. Modeled coherence is plotted using an f value of 1 and elastic thickness values of 40 km (dash-diamond line), 50 km (dashed line) and 60 km (solid line).

marginally above 0.5, and thus results for this area may be somewhat less reliable.

4.2. Geology

All four regions contain surface units interpreted to be either Hesperian or Amazonian lava flows or sediments [33]. While Hesperian and Amazonian plains units cover the lowlands [33–35], crater counts for the lowlands basement based on analyses of high-resolution MOLA maps show that they are comparable in age (Noachian) to the southern highlands [36,37]. A Noachian basement is also supported by the remnants of large craters and multi-ring basins [e.g. 38]. While the age range across the lowlands basement appears to be relatively small, preliminary work suggests that there are some variations in the density of buried features [Frey, pers. comm. 2005]. For example, west of Olympus Mons and north of Alba Patera (which incorporates our region 2: Arcadia Planitia), there were almost no buried craters >50 km, in contrast to other regions such as regions 3 and 4 (Acidalia Planitia) and Utopia where there are buried craters present. Region 2 may be relatively younger due to the smaller buried crater population. Alternatively, the absence of buried features could also be due to very great thickness of cover.

It is possible that these four regions may have higher topographic power (and subsequently better determined admittance spectra) than other lowland regions because they experienced less erosion due to composition. Lower amounts of deposition may also have an effect on the topography.

5. Discussion

5.1. Elastic thickness

For the four regions, our estimated values of elastic thickness overlap within the errors. Overall, the elastic thickness estimates range from 0 to 45 km. Using parameter values and assumptions following Kiefer [39], this corresponds to a heat flux >50 mWm^{-2} when the regional topography was emplaced. These small estimates of elastic thickness are consistent with estimates found for other Noachian age terrains (Fig. 4) [e.g. 9,12,39] and may reflect the high heat flow expected early in Mars' history. We do note however that unlike McGovern [9,10], Kiefer [39] does not correct his heat flux conversions for plate curvature resulting in slightly higher hear flux values. McGovern [9,10] convert elastic thickness into heat flux estimates using the approach developed by McNutt [31], with a specific set of assumptions, including a crustal thickness of 50 km and strain rates between 10^{-19} and 10^{-16} s^{-1}. This method yields heat fluxes of approximately 30–60 mW/m^2 for elastic thicknesses of 0 to 45 km.

Nimmo [12] used admittance to obtain elastic thickness estimates that are generally higher that our values (37 to 89 km), but his study area was considerably larger and may have been influenced by diverse geologic terrains. We note that all of McGovern et al.'s [9,10] Noachian terrain elastic thickness estimates were derived using a top loading model and are therefore smaller than our bottom loading model estimates. Petit and Ebinger [40] discuss the results of numerous terrestrial admittance studies and point out that the T_e values obtained from top and bottom loading models for the same regions typically differ significantly, with bottom loading models giving larger values. They argue that in their terrestrial study region, the thickness of the

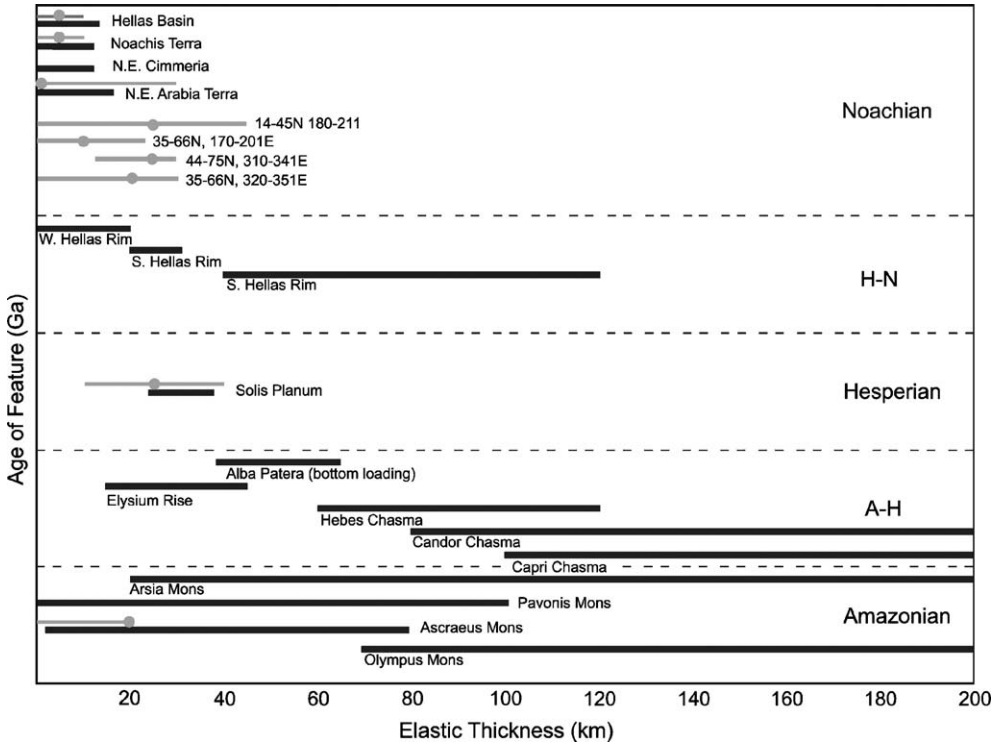

Fig. 4. Best fit elastic thickness versus surface age for the highlands of Mars [9] are shown as black dots with the allowable error range indicated by a black line. Similarly, our T_e estimates obtained for the lowlands are shown in grey. In order to test the multitaper approach on Mars, estimates for the southern highlands are also shown in grey. The age divisions correspond to the Noachian, Hesperian, and Amazonian epochs (in order of decreasing age); the remaining two subdivisions are used to identify features that exhibit surface unit ages spanning two epochs. Within a given subdivision, vertical positions give an approximate indication of the relative surface ages of highland features, based on crater counts [e.g., 48,49] and geologic mapping, although the development of a given pair of features may have overlapped in time.

seismogenic layer is most consistent with T_e values derived from bottom loading model fits.

As discussed in Section 4.1, the surficial units in these 4 regions are Hesperian and Amazonian in age. The fact that all regions are much better fit by bottom loads indicates that loading by surface deposits is not a major contributor to the admittance signature. Shallow, surficial units distributed over broad regions may not have been sufficient to disturb the flexural signature, or may be essentially isostatically compensated.

Prior to this study, the only estimate of northern lowlands T_e (~100 km) [14] came from forward models of the Utopia basin. However, recent and more detailed forward models of Utopia and Hellas (which include basin loading over time), assume a small T_e at the time of formation [41].

5.2. Crustal thickness and depth of compensation

All four regions are best fit by a bottom loading model (in which the crustal thickness is set to 50 km). For these regions we estimate best fit apparent depth of compensation values between 50 and 120 km respectively. The apparent depth of compensation likely represents a deeper density interface below the crust mantle boundary.

Previous studies [e.g. 14,28] estimate that the northern lowlands crust is about 25 km thinner than that of the highlands. Wieczorek and Zuber [29] estimate the average thickness of the entire Martian crust to lie between 33 and 81 km. Neumann et al. [28] estimate crustal thicknesses within the range of ~20–40 km for regions 1 and 2 and ~17–30 km for regions 3 and 4. Assuming a crustal thickness value of 20 km (similar to estimates obtained for our regions 1 and 3 by Neumann et al. [28] rather than a global average of 50 km, results in a best fit apparent depth of compensation estimate ~10 km lower. Using the smaller crustal thickness value does not affect the T_e estimate.

5.3. Implications for northern lowlands formation

Models for the creation of the lowlands implement mechanisms which vary from internal processes, including first order mantle convection [1,2,38] or plate tectonics [e.g. 3,8] to external processes, such as single [4] or multiple [5] large impacts.

The small T_e estimates obtained for the northern lowlands may imply either that the lowlands formed early in the history of Mars, when thermal gradients were high, or that significant heating occurred later, such as above a plume [2,42]. Our T_e estimates are consistent with formation of the northern lowlands via degree one convection, crustal overturn (which also requires a mechanism such as degree one convection to localize the product of a second melt source region in the northern lowlands [43]. Each of these mechanisms implies relatively low T_e values at the time of formation. The bottom loading may have originally been related to one or more mantle plumes. Additionally, significant pressure-release melting may have created a low-density residuum layer that could also contribute to a bottom load.

Our T_e estimates are inconsistent with a plate tectonic model of formation. In terrestrial oceanic basins a progression of elastic thickness with age is observed, whereas we find no such progression in our limited study of 4 regions. Until higher resolution gravity data is acquired, it is not possible to establish a definitive progression in lithospheric parameters of the northern lowlands. However, the absence of age differences in the lowlands, contradicts the plate tectonic hypothesis.

5.4. Implications for northern lowlands relative lack of magnetism

While crustal remnant magnetization is very strong in much of the highlands, Acuna et al. [44] found only a few small amplitude anomalies in the lowlands. More recent research [45] shows that while there are more magnetic anomalies in the northern lowlands than previously thought, there are still fewer magnetic anomalies with generally lower amplitudes in the lowlands than in the southern highlands. The scarcity of magnetic anomalies in the lowlands remains unexplained. One hypothesis is that a degree 1 plume beneath the lowlands caused lower crustal heating and erosion [2]. Another is that hydrothermal circulation due to an ancient ocean caused demagnetization [46,47]. Alternatively volcanic resurfacing and burial of the ancient crust to large depths could also have removed magnetization.

A variety of studies suggest that the bulk of the crust, the dichotomy boundary and the dynamo were all created in the early Noachian [14,47]. In addition, crater counts for the northern lowlands basement based on analyses of high-resolution MOLA maps show that they are comparable in age to the southern highlands [36,37]. The low T_e values also imply that the flexural signature of the northern lowlands was determined early in Mars' history. As suggested by the similar basement ages, the overlap between our T_e estimates of the northern lowlands and the southern highlands supports the formation of both regions within a short time period.

Each of the 4 regions in our study has a good admittance signature (Fig. 3a,b,c,d), low pedestal crater density

[33] and relatively high magnetization [45] for the lowlands areas. Although there is one lowlands region (~60N 30E) with relatively high magnetization that has neither a good admittance signature, nor low pedestal crater density, we speculate that the lack of erosion and associated hydrothermal circulation could be responsible for these three characteristics (admittance, crater density, magnetization). Low erosion could explain the smaller number of pedestal craters and improve the power in the topography. If these areas experienced lower hydrothermal circulation, it may explain the higher levels of magnetization. However, it may be possible that regions of apparently unmagnetized crust in the lowlands formed after dynamo shut down.

6. Conclusions

We have analyzed MGS and Odyssey gravity and topography data for the northern lowlands of Mars, using a multitaper method to reduce the bias of eroded topography. Estimates of admittance spectra were compared with predictions from flexural models to obtain estimates of the elastic lithosphere thickness T_e. Estimates of elastic thickness were obtained for four regions. The number of elastic thickness estimates was limited by the lack of power in the topography in most areas of the northern lowlands. Best fit elastic thickness values ranged between 0 and 45 km. These small estimates are similar to previous studies of the southern highlands and are consistent with formation in the Noachian when heat flow was high. However later reheating cannot be ruled out. Most proposed mechanisms of lowlands formation predict low values of T_e, with the exception of plate tectonics, which predict a range of T_e values in the lowlands. The similarity in T_e estimates between the Noachian highlands and lowlands basement suggests that both regions of the crust formed at similar times. The bottom loading signature is also consistent with loading via a plume or plumes, or low-density mantle residuum. The paucity of crustal magnetization in the lowlands is thus more likely a result of demagnetization than formation following shut down of the dynamo.

Acknowledgements

We thank D. McKenzie for providing his multitaper code and H. Frey for helpful discussions on crater counts in the northern lowlands. We also thank A. Konopliv for providing the MGS95J gravity field. We also wish to thank Patrick McGovern and an anonymous reviewer for their thorough, helpful, and timely reviews. This work was supported by a Mars Data Analysis grant to S. Smrekar. T. Hoogenboom was supported by a National Academies NASA Post-Doctoral Research Associateship.

References

[1] D.U. Wise, M.P. Golombek, G.E. McGill, The tectonic evolution of Mars, J. Geophys. Res. 84 (1979) 7934–7939.
[2] S.E. Zhong, M.T. Zuber, Degree-1 mantle convection and the crustal dichotomy on Mars, Earth Planet. Sci. Lett. 189 (2001) 75–84.
[3] A. Lenardic, F. Nimmo, L. Moresi, Growth of the hemispheric dichotomy and the cessation of plate tectonics on Mars, J. Geophys. Res. 109 (2004) E02003, doi:10.1029/2003JE002172.
[4] D.E. Wilhelms, S.W. Squyres, The Martian hemispheric dichotomy may be due to a giant impact, Nature 309 (1984) 138–140.
[5] H. Frey, R.A. Schultz, Large impact basins and the megaimpact origin for the crustal dichotomy on Mars, Geophys. Res. Lett. 15 (1988) 229–232.
[6] V.R. Baker, R.G. Strom, V.C. Gulick, J.S. Kargel, G. Komatsu, V.S. Kale, Ancient Oceans, ice sheets and the hydrological cycle on Mars, Nature 352 (1991) 589.
[7] T.J. Parker, R.S. Sauders, D.M. Schneeberger, Transitional morphology in west Deuteronilus Mensae, Mars—implications for modification of the lowland/upland boundary, Icarus 82 (1989) 111–145.
[8] N.H. Sleep, Martian plate tectonics, J. Geophys. Res. 99 (1994) 5639–5655.
[9] P.J. McGovern, et al., Localized gravity/topography admittance and correlation spectra on Mars: implications for regional and global evolution, J. Geophys. Res. 107 (E12) (2002) 5136, doi:10.1029/2002JE001854.
[10] P.J. McGovern, et al., Correction to "localized gravity/topography admittance and correlation spectra on Mars: implications for regional and global evolution", J. Geophys. Res. 109 (E07007) (2004), doi:10.1029/2004JE002286.
[11] D. McKenzie, D.N. Barnett, D. Yuan, The relationship between Martian gravity and topography, Earth Planet. Sci. Lett. 195 (2002) 1–16.
[12] F. Nimmo, Admittance estimates of mean crustal thickness and density at the Martian hemispheric dichotomy, J. Geophys. Res. 107 (E11) (2002) 5117, doi:10.1029/2000JE001488.
[13] S.E. Smrekar, G.E. McGill, C.A. Raymond, A.M. Dimitriou, Geologic evolution of the Martian dichotomy in the Ismenius area of Mars and implications for plains magnetization, J. Geophys. Res. 109 (2004) E11002, doi:10.1029/2004JE002260.
[14] M.T. Zuber, et al., Internal structure and early thermal evolution of Mars from Mars Global Surveyor topography and gravity, Science 287 (2000) 1788–1793.
[15] C.J. Swain, J.K. Kirby, The effect of 'noise' on estimates of elastic thickness of the continental lithosphere by the coherence method, Geophys. Res. Lett. 30 (2003) 11, doi:10.1029/2003GL017070.
[16] A.S. Konopliv, C.F. Yoder, E.M. Standish, D-N. Yuan, W.L. Sjogren, A global solution for the Mars static and seasonal gravity, Mars Orientation, Phobos and Deimos Masses, and Mars Ephemeris, Icarus 1 (182) (2006) 23–50.
[17] D.E. Smith, et al., The global topography of Mars and implications for surface evolution, Science 284 (1999) 1495–1503.
[18] P. Wessel, W.H.I. Smith, Free software helps map and display data, Eos, Trans. - AGU 72 (1991) 441.

[19] D.W. Forsyth, Subsurface loading and estimates of the flexural rigidity of continental lithosphere, J. Geophys. Res. 90 (1985) 12623.
[20] L.M. Dorman, B.T.R. Lewis, Experimental isostasy, I: theory of the determination of the earth's isostatic response to a concentrated load, J. Geophys. Res. 75 (1970) 3357–3365.
[21] D. McKenzie, D. Fairhead, Estimates of the effective elastic thickness of the continental lithosphere from Bouguer and free air gravity anomalies, J. Geophys. Res. 102 (B12) (1997) 27523–27552.
[22] D.J. Thomson, Spectrum estimation and harmonic analysis, Proc. IEEE 70 (1982) 1055–1096.
[23] D. Slepian, Prolate spheroidal wave functions, Fourier analysis and uncertainty, V. The discrete case, Bell Syst. Tech. J. 57 (1978) 1031–1042.
[24] D.B. Percival, A.T. Walden, Spectral Analysis for Physical Applications, Multitaper and Conventional Univariate Techniques, Cambridge University Press, New York, 1993, pp. 1–19.
[25] F.J. Simons, M.T. Zuber, J. Korenaga, Isostatic response of the Australian lithosphere: estimation of effective elastic thickness and anisotropy using multitaper spectral analysis, J. Geophys. Res. 105 (2000) 19,163–19,184.
[26] M. Perez-Gussinye, A.R. Lowry, A.B. Watts, I. Velicogna, On the recovery of effective elastic thickness using spectral methods: examples from synthetic data and from the Fennoscandian Shield, J. Geophys. Res. 109 (2004) B10409, doi:10.1029/2003JB002788.
[27] A.T. Walden, E.J. McCoy, D.B. Percival, The effective bandwidth of a multitaper spectral estimator, Biometrika 82 (1) (1995) 201–214.
[28] G.A. Neumann, M.T. Zuber, M.A. Wieczorek, P.J. McGovern, F.G. Lemoine, D.E. Smith, Crustal structure of Mars from gravity and topography, J. Geophys. Res. 109 (E08002) (2004), doi:10.1029/2004JE002262.
[29] M.A. Wieczorek, M.T. Zuber, Thickness of the Martian crust: improved constraints from geoid-to-topography ratios, J. Geophys. Res. 109 (E01009) (2004), doi:10.1029/2003JE002153.
[30] R.J. Banks, R.L. Parker, S.P. Huestis, Isostatic compensation on a continental scale: local versus regional mechanisms, Geophys. J. R. Astron. Soc. 51 (1977) 431–452.
[31] M.K. McNutt, Influence of plate subduction on isostatic compensation in northern California, Tectonics 2 (1983) 399–415.
[32] M.A. Wieczorek, R.J. Phillips, Lunar multiring basins and the cratering process, Icarus 139 (1999) 246–259.
[33] K.L. Tanaka, J.A. Skinner and T.M. Hare, Geologic Map of the Northern Plains of Mars, Scientific Investigations Map 2888, 2005.
[34] D.H. Scott and K.L. Tanaka, Gelogic map of the western equatorial region of Mars, U.S. Geol. Surv. Misc. Invest. Map, I-1802-A, 1986.
[35] R. Greeley and J.E. Guest, Geological map of the eastern equatorial region of Mars, U.S. Geol. Survey Misc. Invest. Map, I-1802-B, 1987.
[36] H.V. Frey, J.H. Roark, K.M. Shockey, E.L. Frey, S.E.H. Sakimoto, Ancient lowlands on Mars, Geophys. Res. Lett. 29 (2002), doi:10.1029/2001GL013832.
[37] H.V. Frey, Impact constraints on, and a chronology for, major events in early mars history, J. Geophys. Res. (2006), doi:10.1029/2005JE002449.
[38] G.E. McGill, A.M. Dimitriou, Origins of the Martian global dichotomy by crustal thinning in the late Noachian or early Hesperian, J. Geophys. Res. 95 (1990) 12595–12605.
[39] W.S. Kiefer, Gravity evidence for an extinct magma chamber beneath Syrtis Major, Mars: a look at the magmatic plumbing system, Earth Planet. Sci. Lett. 222 (2004) 349–361.
[40] C. Petit, C. Ebinger, Flexure and mechanical behavior of cratonic lithosphere: gravity models of the East African and Baikal Rifts, J. Geophys. Res. 15 (2000) 19,151–19,162.
[41] M. Searls, W.B. Banerdt, R.J. Phillips, Utopia and Hellas Basins, Mars: twins separated at birth, J. Geophys. Res. (2006), doi:10.1029/2005JE002666.
[42] D. Breuer, D.A. Yuen, T. Spohn, S. Zhang, Three dimensional models of Martian mantle convection with phase transitions, Geophys. Res. Lett. 25 (1998) 229–232.
[43] L.T. Elkins-Tanton, P.C. Hess, E.M. Parmentier, Possible formation of ancient crust on Mars through magma ocean processes, J. Geophys. Res. 110 (2005) E12S01, doi:10.1029/2005JE002480.
[44] M.J. Acuna, et al., Global distribution of crustal magnetization discovered by the Mars Global Surveyor MAG/ER experiment, Science 284 (1999) 700–793.
[45] D.L. Mitchell, R.J. Lillis, R.P. Lin, J.E.P. Connerney, M.H. Acuna, A global map of Mars' crustal magnetic field based on electron reflectometry, submitted for publication.
[46] S.C. Solomon, and et al., Why are there so few magnetic anomalies in Martian lowlands and basins? In Lunar and Planetary Science XXXIII, Abstract #1382, Lunar and Planetary Institute, Houston (CD-ROM), 2003.
[47] S.C. Solomon, et al., New perspectives on ancient Mars, Science 307 (2005) 1214–1220.
[48] G. Neukum, K. Hiller, Martian ages, J. Geophys. Res. 86 (1981) 3097–3121.
[49] J.B. Plescia, R.S. Saunders, The chronology of the Martian volcanoes, Proc. Lunar Planet Sci. Conf. 10th, 1979, pp. 2841–2859.